International Journal of Signal Processing, Image Processing and Pattern Recognition
Vol.8, No.12 (2015), pp.297-308
http://dx.doi.org/10.14257/ijsip.2015.8.12.28

Signal Feature Extraction of GMI Sensor in Longitudinally Excitated Amorphous Wire and Its Application in Target Detection

Xiusheng Duan[1] and Jing Xiao[2]

[1, 2]*Ordnance Engineering College, Hebei, Shijiazhuang, 050003, China*
sjzdxsh@163.com, xiao_jing801@163.com

Abstract

In order to expand the dynamic range of the GMI sensor in longitudinally excitated amorphous wire and improve its precision, waveforms of the GMI sensor are analyzed on the background of weak magnetic field measurement. Then three features extraction methods are studied in detail. According to the advantages and disadvantages of different methods, an improved method which combines the energy features of the wavelet decomposition and the amplitude features is proposed. First, fit the amplitude change ratio curve respectively with Gaussian function and polynomial function, which not only solves the problem of nonlinearity, but also improves the measurement accuracy. Considering the difference of signals' in-pulse features at different positions, the 'db5' wavelet is introduced to decompose the signals. Then the BP neural network trained by the energy features of the wavelet is used to locate the target's approximate position, as a result, the problem of multi-value is solved. At last, experiments of target detection in weak magnetic field prove that the method proposed is effective.

Keywords: *GMI sensor, feature extraction, target detection, wavelet analysis, BP neural network*

1. Introduction

In longitudinally driven amorphous wire, the GMI curve usually has the problems of nonlinearity and multi-value, as is showed in Figure 1, which gives the GMI curves at different excitation frequencies. In the picture, the approximate linear interval is about 2-10 Oe (1 Oe=10^{-4} T) [1]. Generally speaking, in order to reduce the costs and simplify the design, the GMI sensor usually uses the approximate linear interval for measurement [2-3], which, as a result, limits its measurement range and applications.

In military field, weak magnetic measurement is one of the key technologies of geomagnetic navigation. Meanwhile, it's also an important way to detect martial targets such as submarines, ships and armored vehicles passively. Under this circumstance, a larger detective range and a higher sensitivity in sensor are needed. At present, the existed magnetic sensor cannot meet these requirements very well: Hall sensor has a low sensitivity about 1-10^{6} Oe and there is a certain magnetic anisotropy during measurement. The resistance ratio of anisotropic magneto-impedance (AMR) sensor is only about 2%-4%, and the sensitivity of which is less than 10^{-2} Oe. Sensitivity of giant magneto-resistance (GMR) sensor and the fluxgate sensor is approximately10^{-6}-10^{2} Oe, but fluxgate sensor requires very high accuracy in winding the coils of the amorphous wire and processing the signals [4-6]. The SQUID sensor has the highest sensitivity of 10^{-10}-10^{-4} Oe [8], but it can be used only in specific environment because of its large size and vast supporting facilities. On the other hand, GMI sensor has the advantages of far detection distance, low energy consumption, high resolution ratio, fast response speed, easily being maintained and so on [7, 9-11], sensitivity of which has exceeded the GMR sensor and Hall sensor. What's more, comparing with the SQUID sensor and fluxgate

ISSN: 2005-4254 IJSIP

sensor with the same sensitivity, the GMI sensor can be made much smaller. These all make the GMI sensor a hotspot in weak magnetic field.

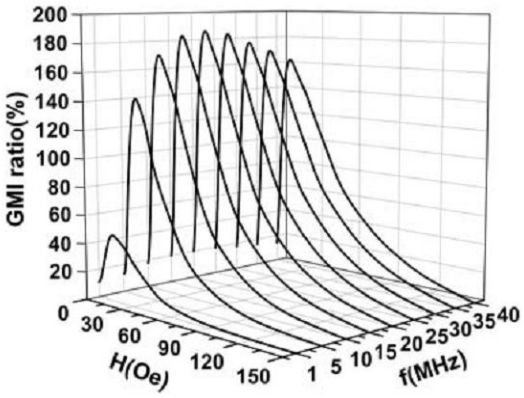

Figure 1. Typical Curve of GMI Effect

Figure 2 shows the relationship between magnetic sensitivity and the detection distance, deriving from the U.S. army research laboratory.

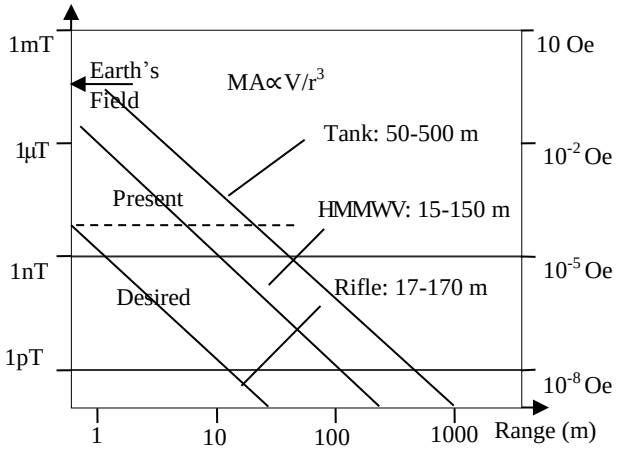

Figure 2. Relationship between Magnetic Field Sensitivity and Detection Distance

When sensitivity of the magnetic field is 10 nT (10^{-4} Oe), sensor's detection distance is about 50 m, when the sensitivity increased to 0.1 nT (10^{-6} Oe), the detection distance is about 158 m. It can be concluded that increasing sensitivity of the sensor plays a very important role in expanding its detection distance. The paper is aiming at increasing GMI sensor's sensitivity and expanding the detection range.

2. Features Detecting

In experiment, a target detecting model is built: a magnet acts as the target, which moves along the specific direction X, as is shown in Figure 3. Each circle is 0.5 cm apart, the GMI sensor locates center of the circles. Outputs of GMI sensor are changing as the magnetic target moves relatively to it. It is assumed that magnetic target approaches the sensor along a specific direction. In the process, the amplitude and waveform of the signal are changing continuously.

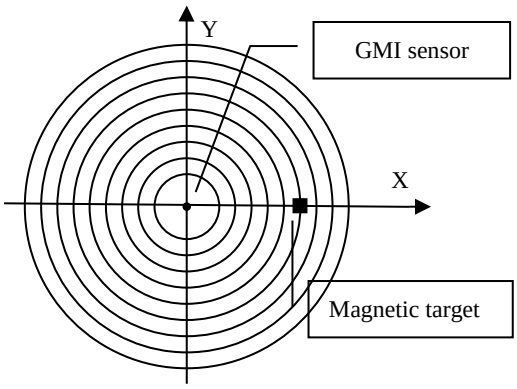

Figure 3. Schematic Diagram of Experiment

Figure 4 gives the experimental environment.

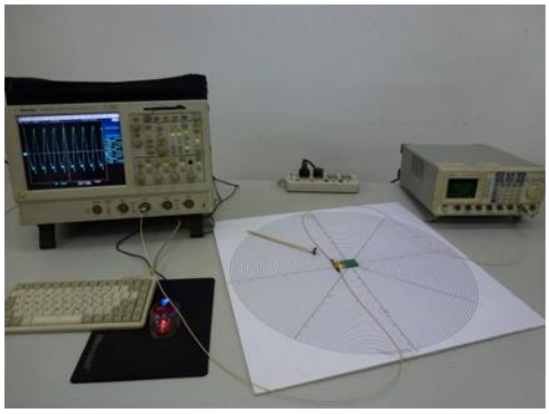

Figure 4. Experiment Equipment

The function generator is INSTEK GFG-3015, which generates the 10 MHz sine signal as excitation for the amorphous wire. Output of the sensor is connected to the Tektronix TDS5104B digital oscilloscope, which samples every image of each position at the frequency of 5 GHz. In order to minimize the influence of the earth's magnetic field and other noise, the GMI sensor is adjusted to ensure the amplitude of the signal is the smallest. Before sampling images, the initial state is defined at the position where the target is far away from the GMI sensor.

Figure 5 shows a few images of several waveforms at six typical positions. It is noted in experiment that there is a position that the amplitude of the signal is the biggest as the target approaches to the sensor.

Further analysis established the next three items. First, because the excitation signal is periodic, the output signal is periodic, too. As the magnetic field outside changes slowly, and the GMI probe can be regarded as an inertial element approximately, so the signal gotten from the data acquisition system is similar to original excitation signal. Second, amplitude of the signal changes continuously, but the change ratio is much different at different intervals. Finally, signal in-pulse features also changes significantly at some positions, which may be caused by the nonlinearity or intermodulation of the device itself [12]. Research shows that there exists intermodulation between the signal coil and the excitation coil of the probe, which cannot be filtered by the low-pass filter, thus the in-pulse features appear, which may lead to more nonlinearity. However, the pulse internal features are not always bad for the signal analysis; it can be used to solve the multi-value problem [12].

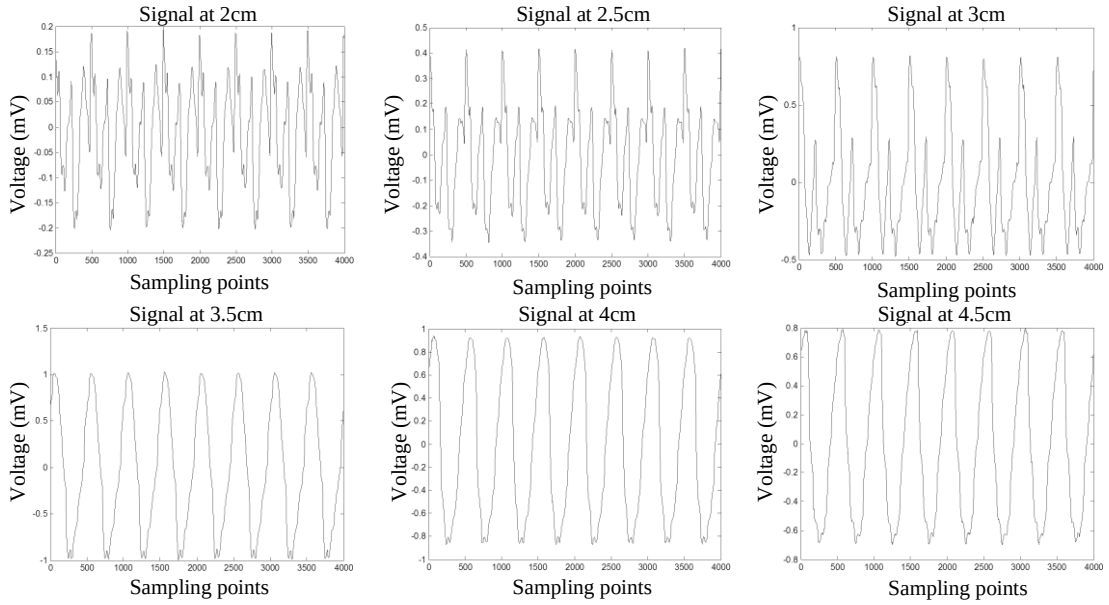

Figure 5. GMI Sensor's Outputs at Positions of 2 cm, 2.5 cm, 3 cm, 3.5 cm, 4 cm and 4.5 cm

In following issues, the amplitude and power change ratio and the wavelet decomposition coefficients of the output signals are discussed, among which, the latter two are based on the characteristics within the pulse.

2.1. Signal Processing based on Amplitude Features

The GMI effect is defined as follows:

$$\frac{\Delta Z}{Z}(\%) = \frac{\left|Z(H_{ex}) - Z(H_{\max})\right|}{Z(H_{\max})} \times 100\ \% \tag{1}$$

$$\frac{\Delta Z}{Z}(\%) = \frac{\left|Z(H_{ex}) - Z(H_{0})\right|}{Z(H_{0})} \times 100\ \% \tag{2}$$

where $Z(H_{max})$ is the impedance under maximum external magnetic field, $Z(H_{ex})$ is the impedance under any external magnetic field, $Z(H_0)$ is the impedance of the initial state. Expression (1) and expression (2) are equal essentially. They both describe the impedance change ratio of the amorphous wire.

In laboratory, the impedance is usually measured by impedance analyzer; the schematic diagram is shown in Figure 6.

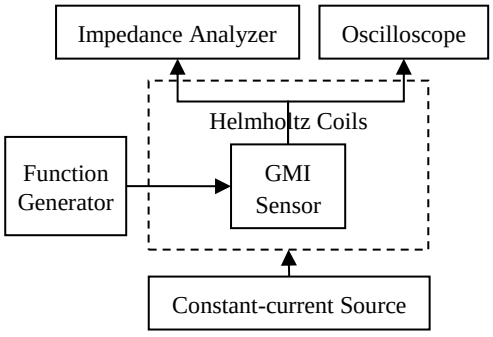

Figure 6. Schematic Diagram for Measuring the GMI Effect

The measurement method in laboratory is visualized and the impedance change can be read immediately, but in the application of target detection, the GMI curve cannot be used directly to explain the relationship between the target distance and the sensor.

An amplitude change ratio of GMI sensor's output at position *i* is defined as $U_r(i)$:

$$U_r(i) = \frac{|U(i) - U(0)|}{U(0)} \times 100\ \% \tag{3}$$

where *Ur(i)* is the signal peak of the waveform at position *i*, *U(0)* is the signal peak at the initial state. The signal peak is the average value of the output signal of *N* periods. The algorithm follows the next 6 steps:

Step1: Record sensor's outputs at the initial state;

Step2: Take the position 2 cm as the starting point, 0.5 cm as the interval of each position, record sensor's output at position *i*;

Step3: For every image, calculate the maximum and minimum of *N* periods, noting as

Step4: Calculate $U_{\max}(i)$ and $U_{\min}(i)$:

$$U_{\max}(i) = \frac{1}{N}\sum_{j=1}^{N} U_{\max\ j}(i) \tag{4}$$

$$U_{\min}(i) = \frac{1}{N}\sum_{j=1}^{N} U_{\min\ j}(i) \tag{5}$$

Step5: Calculate the sensor's amplitude at position *i*;

Step6: Calculate the amplitude change ratio *Ur(i).*

Figure 7 is the curve of the amplitude change ratio. It follows the same law with the GMI effect curve. The further the distance is, the weaker the magnetic field is, and the amplitude and the impedance change ratio follow the same rule, which in turn proves that the amplitude features can present the GMI effect.

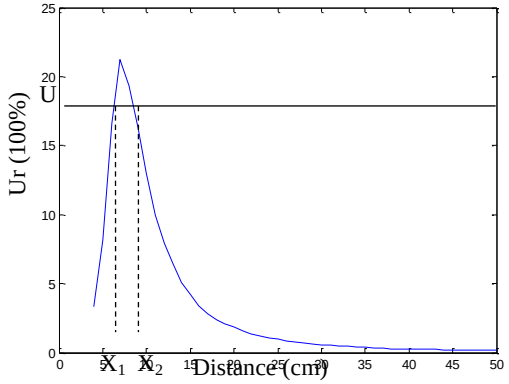

Figure 7. Amplitude Change Ratio of GMI Sensor

The amplitude change ratio can be divided into 3 pats: in the first part, the amplitude change ratio increases gradually with the target distance, reaching the maximum 2126.3%; in the second part, target distance increases while the amplitude change ratio decreases, and during a small period, it changes at an approximate linear rate; in the third part, the amplitude change ratio decreases as well, but the change ratio is slower, finally turns to 0. In the end, the magnetic field generated by the target is very small and the GMI sensor cannot detect it any more.

It needs to be pointed out that in Figure 7, the amplitude change ratio and target's position have the one-to-one correspondence relationship, but if the amplitude change ratio of the GMI sensor is known and the target's position is to be detected, there may be two results. For example, the change ratio at position X_1 and X_2 both are U, when U is used to solve the position, the solution is X_1 or X_2, but one of which is far from the real position. Using it may lead to the wrong result [13].

In order to find a proper expression to describe the curve, fit the curve of amplitude change ratio of GMI sensor on the whole, the result is shown in Figure 8.

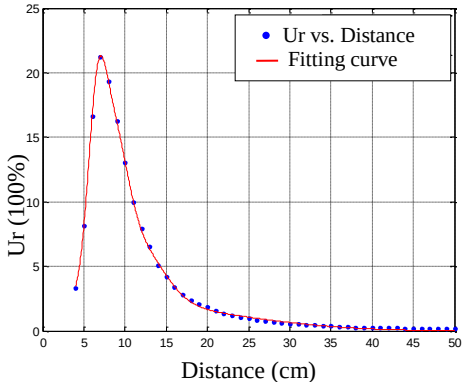

Figure 8. Fitting Curve of GMI Sensor's Amplitude Change Ratio

The fitting curve can be described as:

$$U_r = a_1 e^{-\left(\frac{x-b_1}{c_1}\right)^2} + a_2 e^{-\left(\frac{x-b_2}{c_2}\right)^2} + a_3 e^{-\left(\frac{x-b_3}{c_3}\right)^2} + a_4 e^{-\left(\frac{x-b_4}{c_4}\right)^2} \quad (7)$$

where a_1=9.119, b_1=6.653, c_1=1.627, a_2=5.747, b_2=8.67, c_2=2.714, a_3=6.108×1014, b_3=-416.3, c_3=75.53, a_4=-22.41, b_4=2.621, c_4=3.632. The average error of the fitting curve is 1.245, and the error sum of squares is 0.1886. The fitting precision is relatively high.

Chose several test positions and calculate their amplitude change ratios, then the solutions can be got by using the fitting curve. Table 1 gives the final results.

2.2. Signal Processing based on Power Features

Although using the amplitude features can represent the relationship between the sensor's outputs and target's positions, the features are on the basis of signal's envelope, other features within the pulse cannot be used fully. For this reason, the method based on power features is put forward. It can be calculated by the next steps:

Step1: Repeat the Step1 and Step2 above and record images of the initial state and other positions;

Step2: For each image, find the amplitude *U(n)* of *Num* sampling sites in *N* periods, then calculate *P(i)*:

$$P(i) = \frac{1}{Num} \sum_{n=1}^{Num} |U(n)|^2 \quad (8)$$

Step3: Calculate the power change ratio *Pr(i):*

$$P_r(i) = \frac{|P(i) - P(0)|}{P(0)} \times 100\ \% \quad (9)$$

Figure 9 is the curve of power change ratio.

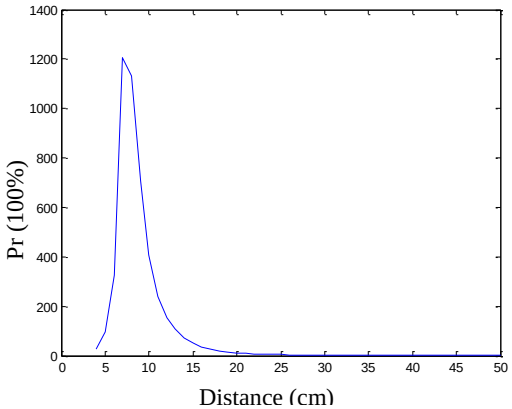

Figure 9. Fitting Curve of GMI Sensor's Power Change Ratio

It can be seen that the curve of power change ratio is similar to the amplitude change ratio, which also can be divided into three parts. But the former changes greater than the later. The linearity of the former is better as well. On the other hand, after the position 25 cm, the power change ratio is close to 0, which means that the GMI sensor is not sensitive to the change of the target's magnetic field any more.

The BP neural network is used to build the relationship of the power features and the target's position. Structure of the network is 47×55×1, in which number 47 is the neurons of input layer, and number 1 is the neurons of the output layer. Number 55 is the neurons of the hidden layer, which is adjusted on basis of the expression below:

$$N \le \text{int}\left(\frac{J(K-1)-(I-1)}{2}\right) \tag{10}$$

where J and I are the neurons of the input and output layer, K is the number of the samples. N is the estimated value of the hidden layer.

Chose some test points and the trained network will give a predictive value of each position. Signal processing results based on the power features are shown in Table 1.

2.3. Signal Processing based on the Coefficients of Wavelet Decomposition

As the wavelet analysis has the characteristic of multi-resolution, local information of the signal can be represented quite well both in time and frequency domain. For a specific signal, the method can adjust the time window and frequency window dynamically [14]. So the wavelet analysis is introduced to process the signal of the GMI sensor. Reference [12] mentions that after the wavelet analysis, the fundamental frequency component of the excitation signal is attenuated to a certain extent. So if these decomposed features are used for measuring, the result is not that good. This also states that the simulation is separate from the practice.

In order to improve the detection precision, the paper improves the wavelet features by combining the fundamental frequency component with the detail coefficients as a feature vector. The BP neural network trained by the feature vector can give the final position accurately.

Decomposing the signal by 'db5' wavelet with 4 layers, there will be the approximate coefficient a_4 and the detail coefficients d_1, d_2, d_3, d_4, as is shown in Figure 10.

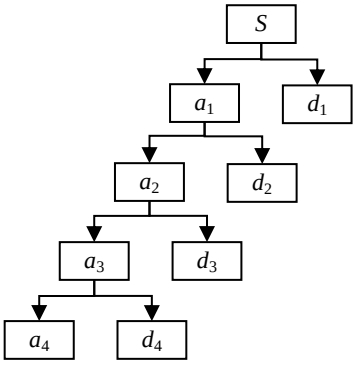

Figure 10. Schematic Diagram of 4 Layers Wavelet Decomposition

Figure 11 gives the results of wavelet decomposition at 6 cm. Considering that frequency of the noise is usually very high, so some coefficients should be taken out. Experiments show that the results are the best when using the approximate coefficient a_4 and the detail coefficient d_1, Therefore, the wavelet features are consist of a_4 and d_1.

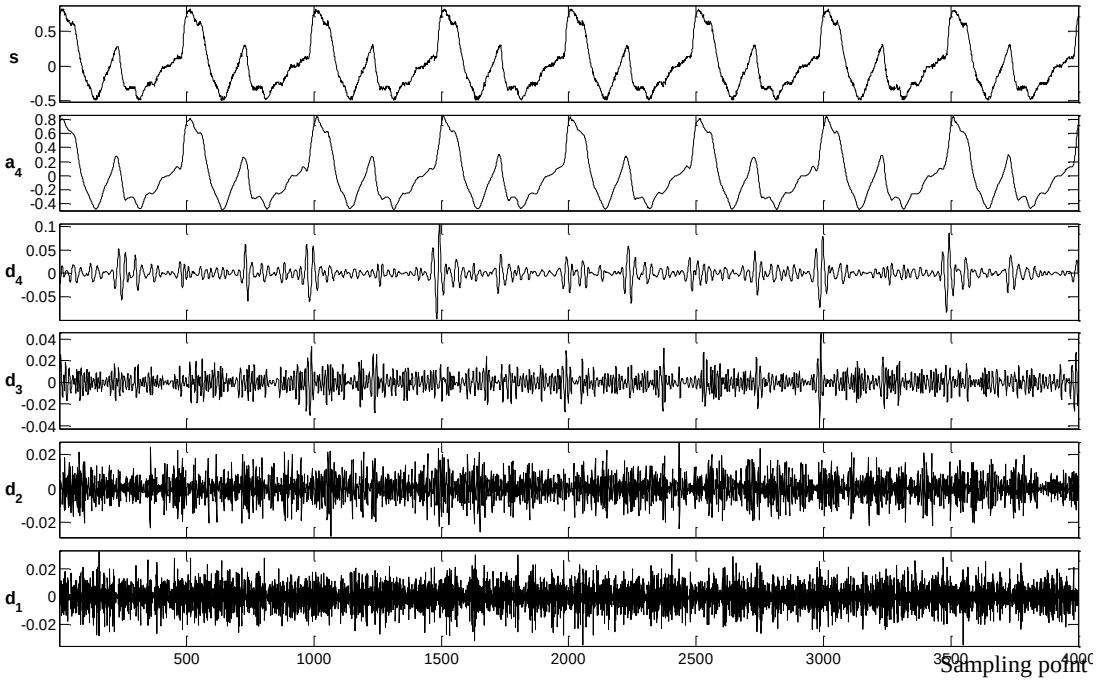

Figure 11. Wavelet Decomposition at 6 cm

Chose a number of test points and calculate their wavelet features, and then put them to the trained BP network, which structure is 2×20×1, the outputs are shown in Table 1.

It is observed that all of the three features mentioned above can give the final positions of test points. In the position 6.5 cm, the deviation is relatively big, which is caused by the multi-value problem in deed: on curve of the amplitude change ratio, the value is the same at the position 6.5 cm and 7.5 cm. Position 7.5 cm is just a predicted value, which is obviously wrong. The precision of the amplitude features become lower after the position 33 cm, which is because after the position, the amplitude change ratio is close to 0, and the GMI sensor is not that sensitive. On the other hand, the results of the power features are very bad at some positions. It doesn't follow a certain rule, which is hard to handle in application. Though position 11.4 cm and 15 cm are in the linear interval, errors of wavelet features of

them are large, which proves that the precision of signal detection with wavelet features is not good, too. So it can be concluded that the amplitude features can satisfy the precision of target detection, but at first, the multi-value problem should be solved.

Table 1. Comparative Results of Discussed Signal Features in Target Detection

Method	Curve fitting method		BP ANN		BP ANN	
Positions (cm)	Amplitude features results (cm)	Relative error	Power features results (cm)	Relative error	Wavelet features results (cm)	Relative error
6.5	7.53	15.85%	7.06	8.62%	5.47	15.8%
9.0	9.20	2.22%	8.66	3.78%	9.69	7.67%
11.4	11.48	0.70%	12.00	5.26%	12.87	12.89%
15.0	15.27	1.80%	15.00	0.00%	16.64	10.93%
18.5	18.94	2.38%	20.09	8.59%	18.91	2.22%
25.5	25.13	1.45%	25.53	0.12%	26.25	2.94%
33.2	29.92	9.88%	33.66	1.39%	32.81	1.18%
39.5	35.67	9.70%	39.46	0.10%	37.98	3.85%

3. Signal Processing Method based on the Amplitude and the Wavelet Features

In order to solve the multi-value problem, a method based on the amplitude and the wavelet features is put forward, which divides the curve of amplitude change ratio into two intervals according to its peak value. In each interval, the change of amplitude is monotonous. If an amplitude feature is corresponding to two positions, BP network trained by the wavelet features will point out the very interval of each signal. Finally, the right position can be obtained using the amplitude features.

What's more, fitting the curve with two intervals can also improve the accuracy of the calculation. The method is an improvement of the least square method, meeting the requirement of the precision proposed by the 'non-linear model' [10]. Next the first interval and the second interval are fitted respectively, which is aiming at found a final fitting model of the GMI sensor's output.

3.1. Fit the First Interval and the Second Interval Respectively

Next, the first interval and the second interval of the amplitude change ratio curve are fitted respectively. It is aimed to build the final fitting model with the amplitude features. Figure 12 (a) and Figure 12 (b) show the fitting results of the two intervals.

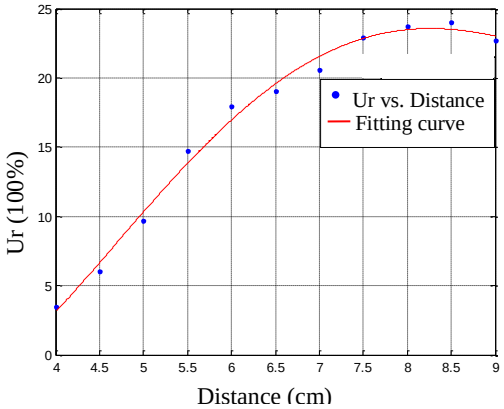

Figure 12 (a). Fitting Results of the First Part of Amplitude Change Ratio

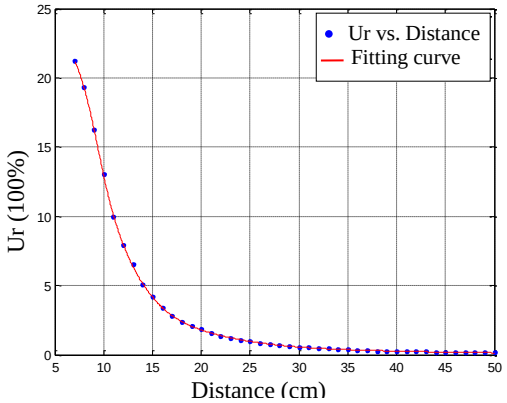

Figure 12 (b). Fitting Results of the Second Part of Amplitude Change Ratio

The first internal's function is as follows:

$$U_r = P_1 x^4 + P_2 x^3 + P_3 x^2 + P_4 x + P_5 \tag{11}$$

where x represents the target's distance. P_1=0.03526, P_2=-1.018, P_3=9.647, P_4=-30.53, P_5=26.96. The average error of the fitting curve is 4.441, and the error sum of squares is 0.8603. The fitting results are not that good because the target is much closer to the sensor and the samples are relatively few.

The second internal's function is as follows:

$$U_r = a_1 e^{-\left(\frac{x-b_1}{c_1}\right)^2} + a_2 e^{-\left(\frac{x-b_2}{c_2}\right)^2} + a_3 e^{-\left(\frac{x-b_3}{c_3}\right)^2} + a_4 e^{-\left(\frac{x-b_4}{c_4}\right)^2} \tag{12}$$

where x represents the target's distance. a_1= 2.564, b_1=2.098, c_1=2.072, a_2= 25.26, b_2=-4.442, c_2=8.652, a_3=4.639×1013, b_3=-979.2, c_3=177, a_4=0.6274, b_4=11.35, c_4=7.978. The average error of the fitting curve is 0.0498, and the error sum of squares is 0.0395. The precision is relatively high.

The final fitting model is presented, which is shown in Figure 13. Left of the peak is the first interval and the right is the second. Then using the wavelet features train the BP network, the output is set to 0 or 1, in which, 0 means the position is in the first internal and 1 means in the second. Thus when an amplitude change ratio is calculated, the network returns 0 or 1. According to it, the final fitting model will give the unique position in the corresponding interval.

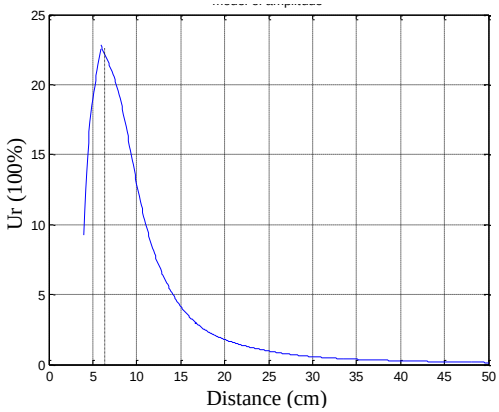

Figure 13. Final Fitting Model of the Amplitude Change Ratio

3.2. Target Detection based on the Final Fitting Model

According to the final fitting model above and the amplitude change ratio of a position, the final result can be calculated. The flow chart is shows in Figure 14:

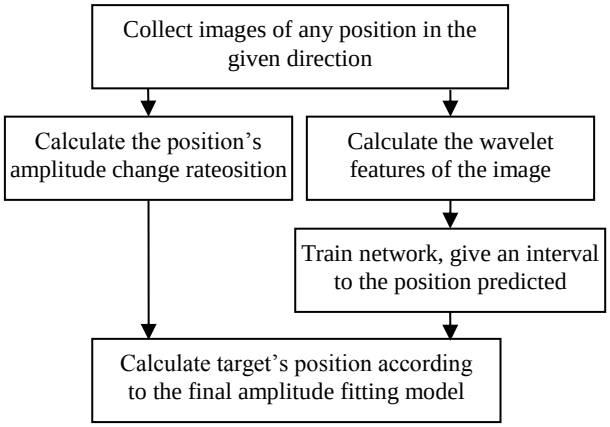

Figure 14. Flow Chart of Target Detection Algorithm based on Final Amplitude Fitting Model

In order to test the method proposed, 10 positions are given in Table 2.

Table 2. Results of Target Detection

Positions	Amplitude change ratio	Output of BP ANN	Results	Relative error
4. 5	3.1258	0	4.58	1.78%
5.5	8.1168	0	5.47	0.55%
6.5	20.9498	0	6.58	1.23%
6.8	21.2632	0	6.75	0.74%
11.4	9.0684	1	11.45	0.44%
15.0	4.05875	1	15.15	1.00%
18.5	2.3166	1	18.29	1.14%
25.5	0.8948	1	25.81	1.22%
33.2	0.4245	1	33.47	0.81%
39.5	0.2758	1	39.81	0.78%

In the table, 4 of the 10 test positions are located left of the amplitude peak and the other 6 are right. It can be seen that the maximum error of the proposed method is about 1.78% and the minimum is 0.44%. Comparing Table 2 with Table 1, it also can be observed that the precision that fitting the amplitude change ratio with two internals is much better than the one which fits the curve on the whole. What's more, for much further positions, the former method has a better precision, too.

4. Conclusions

Method of GMI sensor's signal detection is discussed in the paper. It analyzes the signal features of the GMI sensor and compares different methods to detect them, then on basis of it, the method which combines the energy feature of wavelet decomposition and the amplitude feature is proposed. With it, the nonlinear and the multi-value problem are solved. Experiments of target detection in weak magnetic field show that the precision is within 1.78%, proving that the method is effective. Comparing with the traditional method of signal processing of GMI sensor, the method proposed improves not only the precision of the sensor, but also the dynamic measurement range. It is the foundation of detecting target at any directions.

References

[1] L. Chen, Y. Zhou, C. Lei and ZM. Zhou, "Giant magneto-impedance effect and voltage response in meander shape Co-based ribbon", Appl Phys A, vol. 98, **(2010)**.
[2] J. Yanwei, F. Jiancheng, W. Sansheng and H. Xuegong, "Design of Magnetic Sensor Based on the Asymmetric Giant Magneto-impedance Effect in Amorphous Alloys", CHINESE JOURNAL OF SENSORS AND ACTUATORS, vol. 24, no. 2, **(2011)**.
[3] Y. Geliang, B. Xiongzhu and S. Xiaojun, Fe-based Amorphous Ribbon Weak, "Magnetic Sensor Based on Longitudinal Excitation", Journal of Nanjing University of Science and Technology, vol. 3, **(2011)**.
[4] T. Das and S. Mandal, "An embedded magnetic field sensing device utilizing giant magneto-impedance (GMI) effect", 2012 Sixth International Conference on Sensing Technology, Montreal, Canadian, **(2012)** April 17-21, pp. 102-107.
[5] S. N. Nejad, A. A. Fomani, R. R. Mansour, "Multilayer Giant Magneto-impedance Sensor for Low Field Sensing", IEEE Transaction on Sensors, **(2013)**.
[6] B. Binghao, Z. Yadong and W. Weizhi, "Study on New Magnetic Sensor Utilizing Giant Magneto-impedance Effect in Amorphous Ribbon", Instrument Technique and Sensor, vol. 9, **(2008)**.
[7] H. Xiping, "Sensors and magnetic amorphous wire impedance detection method based amorphous wire impedance effect", Chinese Patent: CN201010240587, **(2010)** May.
[8] S. NazariNejad, A. Akhavan Fomani and R. Mansour, "Giant Magneto-Impedance Thin Film Magnetic Sensor", IEEE TRANSACTIONS ON MAGNETICS, vol. 49, no.7, **(2013)**.
[9] X. Weinan, M. Guangcheng and W. Qiyong, "Mathematical Modelling of GMI Sensor with Double-core Structure", The 11th IEEE International Conference on Electronic Measurement & Instruments, Harbin, China, **(2013)** August 16-19, pp. 901-904.
[10] A. A. Kaya, "Prediction of giant magneto-impedance effect in amorphous glass-coated micro-wires using artificial neural network", Journal of Inequalities and Applications, vol. 216, **(2013)**.
[11] CHAI Xiu-li and ZHANG Yan-yu, "Research progress of magnetic sensors based on giant magnetoimpedance effect", Transducer and Microsystem Technologies, vol. 12, **(2011)**.
[12] Z. Lei and P. Zhongming, "Wavelet analysis of data from GMI magnetic sensors", JOURNAL OF NATIONAL UNIVERSITY OF DEFENSE TECHNOLOGY, vol. 34, no. 4, **(2012)**.
[13] J. XIAO and X. DUAN, "Dianjun TENG. Incentive Optimization Design of GMI Sensors", Applied Mechanics and Materials, vol. 4, **(2014)**, pp. 94-495.
[14] G. Zhi, Principle and Application of Matlab's Wavelet Analysis Toolbox, Defense Industry Press, **(2004)**.

Authors

Xiusheng DUAN, he is born in Shijiazhuang, Hebei provence, China in 1970. He received his doctor's degree form Ordnance Engineering College. He is currently an associate professor in the Ordnance Engineering College. His current research interests include equipment test and fault diagnosis.

Jing XIAO, she is born in Weinan city, Shanxi provence, China in 1989. She got her bachelor's and master's degree in the Ordnance Engineering College. Now she is pursuing her doctor's degree in Ordnance Engineering College. Her research interests concentrate on equipment test and fault diagnosis.

